X-ray Absorption Fine Structure Study of the Active Site of Zinc and Cobalt Carboxypeptidase A in Their Solution and Crystalline Forms†

Ke Zhang*,‡ and Britton Chance‡,§

Biostructures Institute, University City Science Center, and Department of Biochemistry and Biophysics, University of Pennsylvania, Philadelphia, Pennsylvania 19104

David S. Auld,∥,⊥ Kjeld S. Larsen,∥ and Bert L. Vallee∥

Center for Biochemical and Biophysical Sciences and Medicine and Department of Pathology, Harvard Medical School, Brigham and Women's Hospital, 250 Longwood Avenue, Boston, Massachusetts 02115

Received July 25, 1991; Revised Manuscript Received October 18, 1991

ABSTRACT: A comparative study on the metal environment of Zn(II)-carboxypeptidase A (ZnCPD) and Co(II)-carboxypeptidase A (CoCPD) in their solution and crystalline forms using the X-ray absorption fine structure (XAFS) technique has been conducted. The first coordination sphere of Zn for ZnCPD in its solution state is found to consist of two distributions of atoms, with four atoms (N or O) located at an average distance of 2.03 ± 0.01 Å and one atom (N or O) located at 2.57 ± 0.04 Å. The four-atom distribution remains the same for ZnCPD in its crystalline state, but the fifth atom is found at 2.36 ± 0.04 Å. Examination of the higher coordination shell, between 2.7 and 4.2 Å, reveals the presence of two imidazoles. Combined with X-ray crystallographic results, a structural model is proposed. The four atoms at an average distance of 2.03 Å are assigned to the two δ_1 nitrogens of His-69 and His-196, one ϵ_1 oxygen of Glu-72, and the oxygen of a coordinated water molecule. The atom at 2.57 Å for ZnCPD in solution is assigned to the ϵ_2 oxygen of Glu-72. The results for CoCPD in solution are similar with the four atoms at an average distance of 2.08 ± 0.01 Å and one atom at 2.50 ± 0.04 Å, which moves to 2.34 ± 0.04 Å in the crystalline enzyme. The intensity of the 3d "pip" peak for CoCPD is consistent with a distorted tetragonal metal geometry for the solution form of the enzyme which is converted to a more pentacoordinated metal site for the crystalline enzyme. The first shell distribution of crystalline CoCPD is quite disordered, which may be largely due to the disorder of His-69 and His-196 as indicated by higher shell analysis. Thus, the XAFS studies show that the metal coordination spheres in the zinc and cobalt enzymes are quite similar in the solution state but differ from their crystalline counterparts. The XAFS studies provide the necessary background for measurement of substrate- and inhibitor-promoted structural changes in the metal coordination sphere of the zinc and other metal-substituted carboxypeptidases in the solution state.

Carboxypeptidase A (ZnCPD)[1] is a zinc enzyme that hydrolyzes the carboxyl-terminal peptide bond in polypeptides and proteins, favoring an aromatic side chain at the terminal residue (Auld & Vallee, 1987). Since the recognition nearly 40 years ago (Vallee & Neurath, 1954) that zinc is a constituent essential to its catalysis, this enzyme has become one of the most popular metalloenzyme targets of biochemical and biophysical studies. Two allotypic variants, Leu and Val, of the α, β, and γ forms of bovine carboxypeptidase have been recognized (Neurath et al., 1970). The primary structures of carboxypeptidase from several different species have been reported, and their putative metal-binding sites have been tabulated (Vallee & Auld, 1990). The crystal structure of bovine ZnCPD, refined to a resolution of 2.0 and 1.54 Å (Reeke et al., 1967; Lipscomb et al., 1968, 1970), in conjunction with the amino acid sequence analysis (Neurath et al., 1970) and chemical modifications (Vallee et al., 1963, 1970), has identified the active site residues. The active site comprises a zinc ion bound to Glu-72, His-69, His-196, and a water molecule in a distorted tetragonal geometry. Ultimately, X-ray crystallographic studies detected that both the ϵ_1 and ϵ_2 oxygens of Glu-72 bind to the zinc ion (Rees et al., 1981, 1983).

Prior to the establishment of the crystallographic structure, a metal, a proton donor, and a base were proposed as the catalytic constituents of carboxypeptidase (Vallee et al., 1963). The X-ray diffraction studies were the basis of the suggestion that Glu-270 acts either to promote general base catalysis of a water molecule or in nucleophilic attack of the substrate carbonyl group and Tyr-248 acts as a proton donor in catalysis (Quiocho & Lipscomb, 1971). Much of the accumulating evidence has supported the role of Glu-270 as a general base/general acid catalyst (Auld & Vallee, 1987; Christianson & Lipscomb, 1989), while the role of Tyr-248 as a proton donor has been placed in doubt by mutagenesis studies (Hilvert et al., 1986). While the crystallographic results have been essential in identifying amino acid residues involved in binding the metal and as an aid to those that may be involved in catalysis, the results of the mutagenesis studies have revealed the limitations and shortcomings of mechanisms solely based

† This research was supported by NIH Grants HL-18708 and RR-01633.

‡ Biostructures Institute.

§ Department of Biochemistry and Biophysics.

∥ Center for Biochemical and Biophysical Sciences and Medicine.

⊥ Department of Pathology.

[1] Abbreviations: ZnCPD, native carboxypeptidase A; CoCPD, cobalt(II)-substituted carboxypeptidase A; FaFF, N-[3-(2-furyl)acryloyl]-L-phenylalaninyl-L-phenylalanine; Im, imidazole; Ac, acetate; Tris, tris(hydroxymethyl)aminomethane; Mops, 3-(*N*-morpholino)propanesulfonic acid; SDS, sodium dodecyl sulfate; DMF, *N*,*N*-dimethylformamide; $Co(Im)_6$ is the $[Co2(Im)_6]Cl_2$ complex; $Zn(Im)_4$ is the $[Zn(Im)_4](ClO_4)_2$ complex; $Zn(NH_3)_4$ is the $[Zn(NH_3)_4](OH)_2$ complex; $Co(Ac)_2$ is the $[Co(H_2O)_4]Ac_2$ complex.

0006-2960/92/0431-1159$03.00/0

on the crystal structure. Furthermore, the rates of hydrolysis by the crystal and solution forms are known to be significantly different. Using a variety of peptide and ester substrates, the rate of catalysis of the crystalline enzyme was found reduced 20–1000-fold (Spilburg et al., 1974, 1977). However, the structures of carboxypeptidase in the solution and crystalline states have not been compared directly.

Among the experimental techniques available, two- or higher-dimensional NMR and X-ray absorption fine structure (XAFS) are the only ones thus far which can examine structure directly in solution. Indeed, the solution structure of metallothionein (Schulze et al., 1988; Messerle et al., 1990) as determined by 2D NMR differs from that reported for the crystalline state (Furey et al., 1987). ^{15}N NMR studies of the solution and crystalline states of α-lytic protease have shown that the catalytic histidine ionizes with a pK_a value 1.1 unit higher for the crystalline state, which explains the absence of a hydrogen bond between the catalytic His and Ser groups in X-ray diffraction studies (Smith et al., 1989).

Recently, XAFS has been used to determine the structural differences around the metal ions of proteins both in solution and in crystalline forms of concanavalin A (Lin et al., 1990, 1991), as well as met-myoglobin (Zhang et al., 1991). The latter study excluded some explanations based on possible artifacts, e.g., preferred orientation for a crystalline sample, radiation damage induced by hydrated electrons generated by the intense radiation, and the presence of high salt concentration in protein crystallization.

Structural differences between proteins in solution and in the crystalline form thus may be a more general feature of protein crystallization than has been suspected. Examination of structural changes in an enzyme can of course be evaluated through their effect on the enzyme's catalytic function. The previously demonstrated reduced catalytic activity of carboxypeptidase in its crystalline state (Spilburg et al., 1974, 1977) and the questions answered by mutagenesis of tyrosine 248 (Hilvert et al., 1986) led to this study of its active site structure in both the solution and crystalline state by XAFS.

Materials and Methods

Enzyme Preparation. Carboxypeptidase A from bovine pancreas prepared according to the method of Cox et al. (1964) was obtained from Sigma Chemical Co., St. Louis, MO (C-0261, lot no. 57F8110), and the α-Val isozyme used here was isolated by a combination of ion exchange and affinity chromatography (Larsen & Auld, 1989). Alternatively, acetone powder from bovine pancreas (Sigma, P-3006, lot no. 40H7215) served as starting material. The procarboxypeptidase A was isolated by DEAE chromatography, and subunit II (pro-ATEEase) was activated by a trace of trypsin, followed by activation of subunit I (the immediate precursor of carboxypeptidase) with activated subunit II (ATEEase) in 1 M $CaCl_2$ (Uren & Neurath, 1972). The affinity-purified enzyme (5–10 mg/mL) was precipitated by dialysis against 0.01 M Mops, pH 7.0. The apoenzyme was prepared from this material by the solid-state method (Auld, 1988). A 2-fold excess of $CoCl_2$ was added to the apoenzyme, and the product, CoCPD, was dissolved to 30–40 mg/mL in 1 M NaCl and 0.01 M Mops, pH 7.0. A small amount of denatured protein was removed by centrifugation, and a microcrystalline enzyme was obtained from the solubilized portion by dialysis against 0.01 M Mops, pH 7.0 (Coleman et al., 1960). This step also eliminates excess cobalt(II) ions. The same schedule of operations was used to prepare microcrystalline ZnCPD except that crystalline material was also obtained from enzyme solubilized in 1 M LiCl and 0.01 M Tris, pH 7.5. Solution samples (2.5–3.0 mM) of ZnCPD and CoCPD were prepared by addition of one volume of 2 M NaCl and 0.01 M Mops, pH 7.0 to wet pellets of crystalline material. The samples were adjusted to 1 M NaCl and 0.01 M Mops, pH 7.0 prior to XAFS measurements. Crystalline samples were immersed in 0.01 M Mops, pH 7.0. Higher salt concentrations will lead to progressive dissolution of the crystals. Our studies of the crystalline enzyme have therefore been done in 10 mM Mops in order to avoid the additional complication of glutaraldehyde cross-linking of the crystals.[2]

The integrity of the sample before and after radiation exposure was assessed by SDS–polyacrylamide gel electrophoresis (Laemmli, 1970) and amino acid analysis (Picotag, Waters Associates) (Bidlingmeyer et al., 1984). Enzymatic actvity was measured under zero-order conditions, using FaFF as the standard substrate (Riordan & Holmquist, 1984). Metal analysis was performed by graphite furnace atomic absorption spectroscopy (Perkin-Elmer, model 5000). Metal-free solutions were prepared as described (Holmquist, 1988), and purified water was used throughout this study (Milli-Q/Milli-RO water purification system, Millipore, Bedford, MA).

Model Compounds. Metal complexes with coordination properties similar to those of the enzyme were used to approximate the backscattering amplitude, as well as central and backscattering phase shifts for the active site of the enzyme. $CoCl_2$, $Co(ClO_4)_2$, $Co(Ac)_2$, $CoCo_3$, $ZnCl_2$, and $Zn(ClO_4)_2$ were purchased from Johnson Matthey Inc., Seabrook, NH ("Puratronic grade"), and imidazole was from Sigma. Crystalline $[Co(Im)_4](ClO_4)_2$ prepared according to the method of Davis and Smith (1971) is characterized by $\epsilon_{562} = 572$ M^{-1} cm^{-1} over the concentration range from 0.2 to 10 mM. The Zn and $Co(Im)_2(Ac_2)$ complexes were prepared according to methods previously described (Horrocks et al., 1980). A spectral titration of $CoCl_2$ (0–60 mM) in 10% imidazole (DMF) documented the formation of $[Co(Im)_6]Cl_2$, with ϵ_{490} = 15.2 M^{-1} cm^{-1} (2–10 mM $CoCl_2$). At higher cobalt concentrations, a spectral shift to 610 nm occurs, presumably due to the formation of $[Co(Im)_4]Cl_2$. The extinction coefficients are based on the metal ion concentration as measured by atomic absorption. XAFS spectra of $[Co(Im)_4](ClO_4)_2$ in acetone and $[Co(Im)_6]Cl_2$, $[Zn(Im)_6]Cl_2$ in DMF were recorded at a metal concentration of 10 mM. The model complex $[Zn(NH_3)_4](OH)_2$ was prepared by precipitation of $Zn(OH)_2$ from $Zn(NO_3)_2$ (Aldrich 23-0006) in 5% ammonium hydroxide followed by redissolution of the $Zn(OH)_2$ in 30% ammonium hydroxide. XAFS spectra of this complex were recorded at zinc concentrations of 10–20 mM.

XAFS Measurements. All XAFS measurements were performed at the National Biostructures PRT Beamline X9-A of National Synchrotron Light Source, Brookhaven National Laboratory. Both Si(111) and Si(220) double crystal monochromators were used for XAFS and the near edge studies, respectively. The crystals were mounted side by side in the monochromator of the beamline. A harmonic rejection mirror eliminated higher order reflection of radiation from the monochromator. The Zn and Co Kα fluorescence, emitted after absorption of the incident X-ray photons, was measured using a 13-element Ge detector and/or a Stern/Heald ioni-

[2] This of necessity leads to comparing the structures of the crystalline and solution enzyme at two different anion concentrations. However, spectroscopic studies of the cobalt enzyme have shown perturbation of the metal coordination sphere by anions occurs only below pH 6 and at anion concentrations > 1 M (Geoghegan et al., 1983; Bicknell et al., 1988).

zation chamber. Most of the data were collected between 100 and 150 K, except for crystalline CoCPD and some cobalt and zinc complexes which were measured at both room and low temperatures. The concentration of the solution enzyme samples for the XAFS measurement was 2–2.5 mM. Crystalline carboxypeptidase was packed in the same sample holder with 0.01 M Mops, pH 7.0. The protein content of the crystals was similar to that of the solution enzyme as determined by the total number of the fluorescence photons detected by the Ge detector. To avoid possible alteration of protein structure, antifreeze, such as ethylene glycol, was not added to any of the samples. The effects of the formation of large ice crystals in the solution, "freeze marks", were minimized by using the Ge detector, which effectively eliminates scattered X-ray photons. Zn- and $Co(Im)_2(Ac)_2$, $Co(Im)_4$, and cobalt acetate and cobalt carbonate were measured in powder form, by spreading them uniformly on Scotch tape. A series of scans for each sample was collected with up to 10^7 effective signal photon counts per point.

Data Reduction and Analysis. XAFS data were reduced following the standard method (Stern & Heald, 1983). The XAFS $\chi(k)$ function was obtained by subtracting the slowly varying atomic background with a cubic spline fit, normalized by a constant edge step, and converted from energy to electron wave number k. A Fourier transform was performed to obtain a pseudoatomic distribution function with respect to radial distance R about the central atom. An isolated single shell $\chi(k)$ was obtained by back transforming a single shell distribution from R space back to k space using a window function. The single shell $\chi(k)$ data were analyzed quantitatively by the least-squares fitting and the ratio methods (Stern & Heald, 1983; Bunker, 1983) using suitable model compounds.

Proper error analysis is acknowledged to be essential for XAFS of dilute systems. The criterion which determines whether a fit should be accepted or rejected is that the quantity Q should be less than or equal to unity (Zhang et al., 1988):

$$Q = \frac{1}{N-P}\sum_{i}^{N}\frac{(\sigma_f^i)^2}{(\sigma_Y^i)^2} \quad (1)$$

where

$$(\sigma_f^i)^2 = (A^i)^2(\phi^i - \phi_f^i)^2 + (A^i - A_f^i)^2 \quad (2)$$

Here A^i and ϕ_i are the experimental amplitude and phase determined at the independent data point of k^i, and A_f^i and ϕ_f^i are the corresponding values of the fit. N is the number of independent data points included within the data range to be modeled (Lee et al., 1981), and P is the number of parameters used in the fit. σ_Y^i comprises measurement errors and the errors introduced by the analysis procedure, which may result mainly from the nontransferability of A and ϕ of the standards to the unknowns. The measurement error can be estimated from the variation of different scans of measurement and the nontransferability error of the standard from the analysis of model compounds of known structure.

It has been demonstrated that the radial distribution function (RDF) can be constructed by using cumulant expansion to extrapolate the low k information which is not available in XAFS (Bouldin, 1984; Crozier et al., 1988; E. A. Stern personal communication). The advantage of the RDF over the fitting method is that the latter may be biased when a wrong model is assumed to fit the data. The major steps of the method are described here. With the single shell $\chi(k)$ data of the unknown and an appropriate model, the physical quantities in the XAFS function, such as the backscattering amplitude and the central and the backscattering phase, can be removed by taking the amplitude and the phase difference between the two. The amplitude ratio and the phase difference are then extrapolated through the low k region using the cumulant expansion. The criterion for the extrapolation is that the cumulant expansion, which usually is used to the fourth order, has to be in a correct functional form to approximate the atomic distribution. This condition may not be met if the displacement of the distribution is extremely large and non-Gaussian. The data then are inverted using a Fourier sine transform, usually with a Gaussian damping factor to minimize artifacts due to truncation of the data in the high k region. The RDF for a model comound is also generated at the same time and compared with the unknown to obtain quantitative results, e.g., to normalize the areas of the RDF.

Assessment of Radiation Damage. The enzyme used here was homogeneous on SDS–polyacrylamide gel electrophoresis, and its amino acid composition and amino-terminal sequence were in agreement with the characteristics of the α-form (Uren & Neurath, 1972). No precipitate was observed in samples exposed to radiation after thawing or during transfer to a storage centrifuge tube. Samples were stored on ice until assessment for radiation damage could be accomplished, usually 2 or 3 days later. Samples subjected to radiation were centrifuged, and the supernatant was analyzed for amino acid composition and enzymatic activity. The amino acid analysis is expected to reveal damaged amino acids from lower stoichiometries and the appearance of degradation products. There was no evidence for radiation damage within the accuracy of the method used in the supernatant fractions. Any precipitated material was not analyzed but represented <5% of the starting material. The process of freezing and thawing carboxypeptidase solutions or even storage (1–4 days) produces some insoluble material.

Results

Model Compounds. The XAFS $\chi(k)$ function obtained from the background subtraction, E to k (photoelectron wave number) conversion, and normalization for $Zn(Im)_4$, $Zn(NH_3)_4$, and $Zn(Ac)_2(Im)_2$ for zinc, and $Co(Ac)_2$, $Co(Im)_6$, and $Co(Ac)_2(Im)_2$ for cobalt are shown in Figure 1A,B. To verify the data analysis procedure, especially the RDF method, $Zn(Ac)_2(Im)_2$ and $Co(Ac)_2(Im)_2$ models were first analyzed using other oxygen and nitrogen models. The Zn or Co ion in $Zn(Ac)_2(Im)_2$ or $Co(Ac)_2(Im)_2$ is coordinated to two oxygens of the two acetates and two nitrogens of the two imidazole rings (Horrocks et al., 1980) and very closely resembles that of the metal coordination environment of carboxypeptidase A (Lipscomb et al., 1968).

In XAFS, nitrogen and oxygen are usually almost indistinguishable when serving as ligands to the metal, due to the small differences in their backscattering amplitudes and phases. We have therefore used either a nitrogen or an oxygen model, respectively, to generate the radial distribution function of $Zn(Ac)_2(Im)_2$ or $Co(Ac)_2(Im)_2$. The XAFS $\chi(k)$ data shown in Figure 1 were transformed between 1 and 12 $Å^{-1}$ in k space, and the single first shell $\chi(k)$ data were obtained by back transforming the first shell atomic distribution with a window of 0.8–2.0 Å in R space. The transforms and the single shell data are not shown here due to space limitations.

The RDF for $Zn(NH_3)_4$, in which the zinc ion is coordinated to four nitrogens at 1.97 Å, and for $Zn(Ac)_2(Im)_2$ are shown in Figure 2A. The radial distribution function of $Zn(NH_3)_4$ at 1.99 Å reflects a systematic error of 0.02 Å in the procedure used to generate the RDF; a systematic error which has been removed in all the following XAFS results. The average

Table I: First Shell Results of Zn and Co Complexes Compared with the X-ray Diffraction Results[a]

		XAFS			diffraction		
sample	standard	N	R (Å)	σ^2 (Å^2)	N	R (Å)	σ^2 (Å)^2
$Zn(Ac)_2(Im)_2$	$Zn(NH_3)_4$	4.0 (4)	2.00 (1)	0.001 (2)	4	1.99	0.000
$Co(Ac)_2(Im)_2$	$Co(Ac)_2$	3.7 (4)	2.02 (1)	0.000 (2)	4	2.03	0.000
$Co(Ac)_2(Im)_2$	$Co(Im)_6$	4.4 (4)	2.04 (1)	0.000 (2)			

[a] The average distance was calculated from Horrocks et al. (1980). The Debye–Waller factor calculated for X-ray diffraction results is the structural disorder. The value in parentheses is ± the error in the last digit.

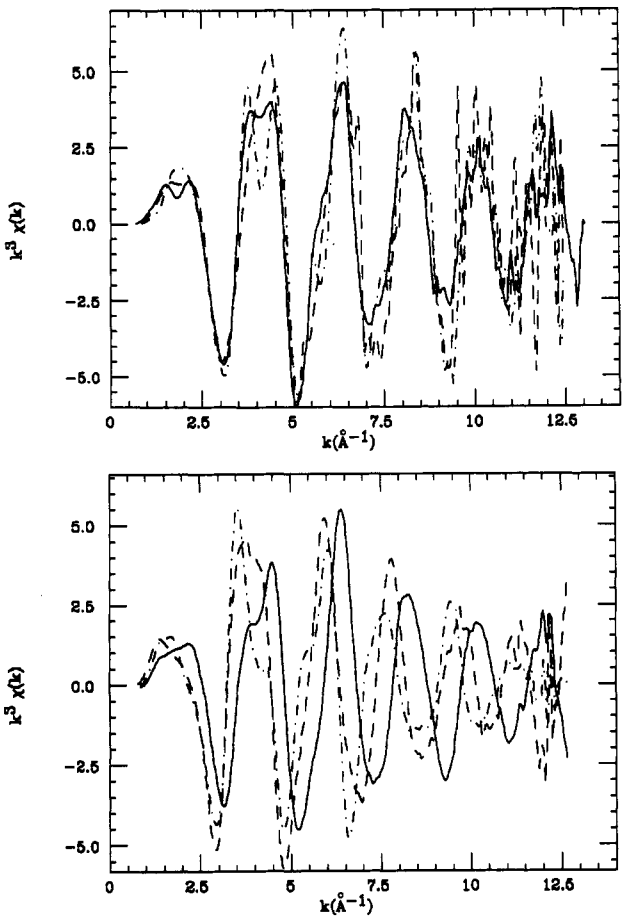

FIGURE 1: (A, top) Zn K-edge XAFS $\chi(k)$ data for selective zinc model compounds, $Zn(Ac)_2(Im)_2$(solid), $Zn(NH_3)_4$ (dash), and $Zn(Im)_4$ (dot-dash). (B, bottom) Co K-edge XAFS $\chi(k)$ data for selective model compounds, $Co(Ac)_2(Im)_2$ (solid), $Co(Ac)_2$ (dash), and $Co(Im)_6$ (dot-dash). The data are weighted with a k^3 factor.

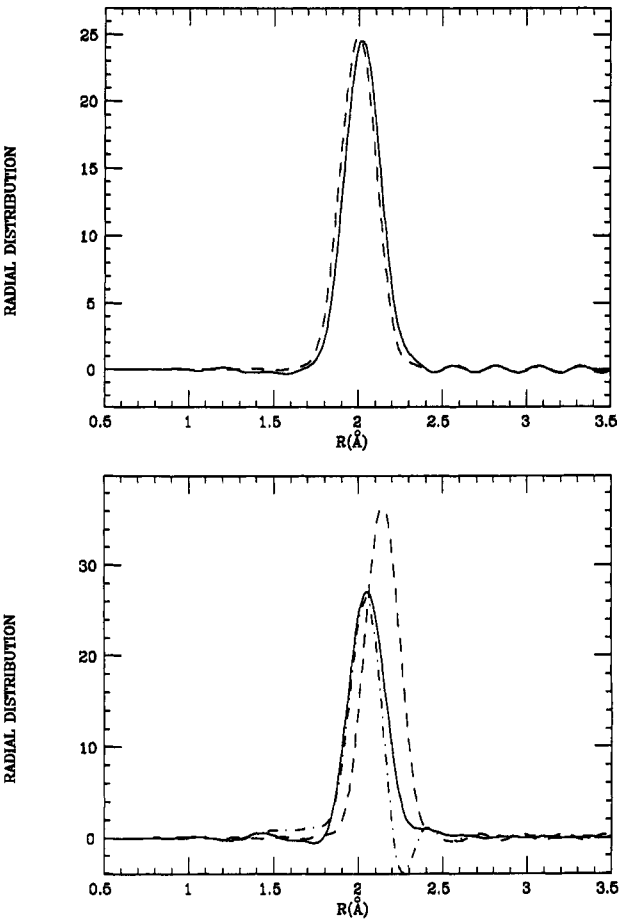

FIGURE 2: (A, top) Radial distribution function (RDF) generated for $Zn(Ac)_2(Im)_2$ using the nitrogen model $Zn(NH_3)_4$ (solid), compared with the RDF of $Zn(NH_3)_4$ (dash). (B, bottom) RDFs generated for $Co(Ac)_2(Im)_2$ using oxygen model $Co(Ac)_2$ (dot-dash) and using the nitrogen model $Co(Im)_6$ (solid), compared with the RDF of $Co(Ac)_2$ (dash). The distributions were artificially broadened by a Gaussian factor of $\sigma_c^2 = 0.01$ Å^2 to reduce the truncation ripple due to limited high k information.

distance of the RDF for $Zn(Ac)_2(Im)_2$ is 2.00 Å. The ratio of the integrated area of the distribution, which is proportional to the first shell coordination number, is about 1.0 between $Zn(Ac)_2(Im)_2$ and $Zn(NH_3)_4$, and the difference between the mean square displacement of the RDF, $\Delta\sigma^2$, is less than 0.001 Å^2. The least-squares fitting method was also used for the analysis of $Zn(Ac)_2(Im)_2$. These results are essentially the same as those for the RDF with about four atoms (nitrogens or oxygens) located at 2.00 ± 0.01 Å (Table I).

The same procedure was used to analyze $Co(Ac)_2(Im)_2$. Figure 2B shows the RDFs of $Co(Ac)_2(Im)_2$ generated using the oxygen $Co(Ac)_2$ and the nitrogen $Co(Im)_6$ models, compared with that of the radial distribution of $Co(Ac)_2$, with six oxygens in the Co first coordination sphere located at an average distance of 2.13 Å. The RDF of $Co(Ac)_2(Im)_2$ modeled by $Co(Ac)_2$ (oxygen) contained 3.7 atoms at 2.02 Å with a small artifact of a negative peak, and the RDF modeled by $Co(Im)_6$ contained 4.4 atoms at 2.04 Å. The average of the two RDFs is a smooth distribution without artifacts containing 4.0 atoms (2 N and 2 O) located at 2.03 Å (not shown). A single-distance least-squares fitting analysis of $Co(Ac)_2(Im)_2$ using the same model compounds gave the same results as those determined by the RDF method (Table I).

The XAFS results for Zn- and Co-$(Ac)_2(Im)_2$ and those of the X-ray diffraction results (Horrocks et al., 1980) are in excellent agreement (Table I). The use of a nitrogen model to simulate a coordination site containing both oxygen and nitrogen will usually yield a slightly higher coordination number and longer interatomic distance, owing to the small difference between the backscattering amplitudes and phases of oxygen versus nitrogen. Conversely, the coordination number will be smaller and the interatomic distance will be shorter using an oxygen model. The combination of the two accurately models a system with a mixture of the two types of atoms. Unless stated otherwise, in the first shell data analysis of carboxypeptidase, all results are derived by using the $Zn(Ac)_2(Im)_2$ and $Co(Ac)_2(Im)_2$ as models of the Zn and

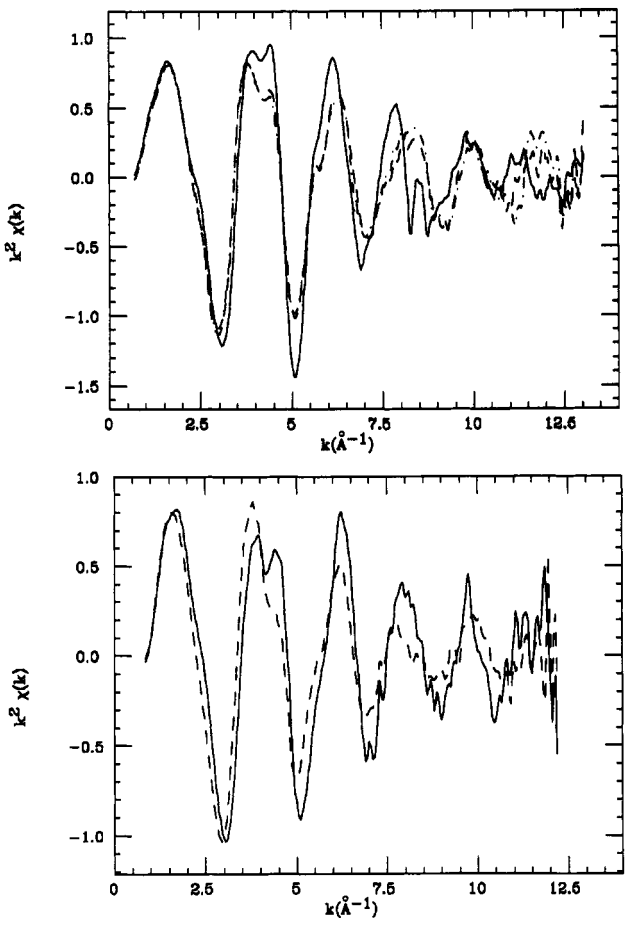

FIGURE 3: (A, top) Zn K-edge XAFS $\chi(k)$ data of ZnCPD in solution (solid) and in crystalline forms grown in NaCl (dash) and LiCl (dot-dash). (B, bottom) Co K-edge XAFS $\chi(k)$ data for CoCPD in its solution (solid) and in crystalline form (dash). The data were weighted with a k^2 factor.

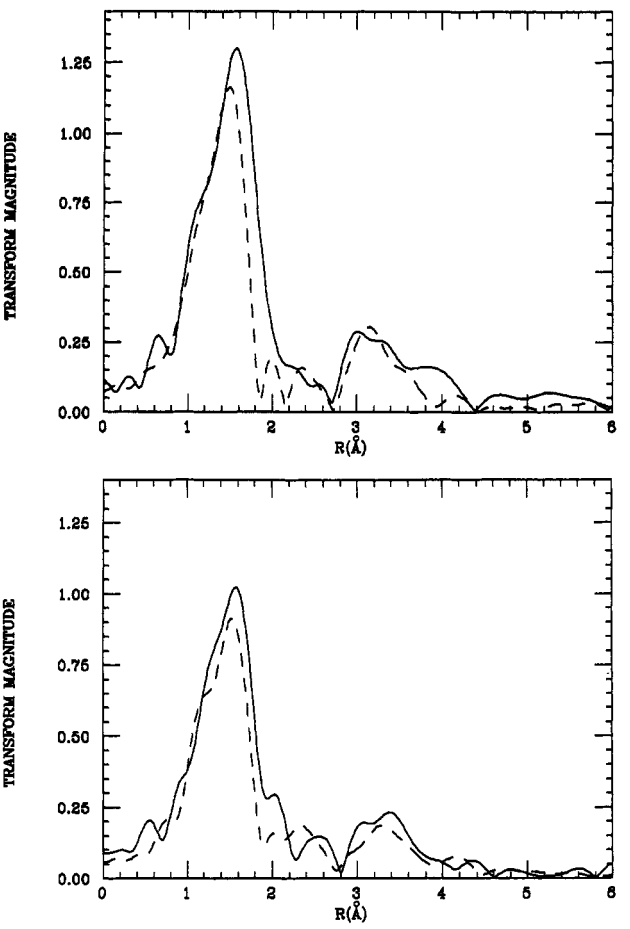

FIGURE 4: Fourier transforms of the XAFS $\chi(k)$ data of the zinc (A, top) and cobalt (B, bottom) enzyme in their solution (solid) and crystalline (dash) forms. The $k^2\chi(k)$ Fourier transform was performed from 1 to 12 Å^{-1}.

Co enzymes, respectively. The results have been checked using other oxygen and nitrogen model compounds.

First Coordination Shell of *Carboxypeptidase.* The XAFS $\chi(k)$ data demonstrate significant differences between the solution and crystalline samples of both the Co and Zn enzymes (Figure 3A,B). The XAFS spectrum for the enzyme crystallized from NaCl is almost identical to that crystallized from LiCl to a k value of 10 Å^{-1} (Figure 3A). Indeed, quantitative data analysis shows that differences between the two forms of crystalline sample are within the limits of error of 0.01 Å for the first shell interatomic distance and within 5% for the coordination number. Therefore, further analyses are shown only for the crystalline sample from NaCl.

The XAFS $\chi(k)$ data for the zinc and cobalt enzymes are Fourier transforms from 1 to 12 Å^{-1} in k space (Figure 4). Again the Fourier transforms of the solution and crystalline samples differ. The Zn and Co enzymes both show a distribution of the first coordination sphere that is broadened more in solution than in the crystalline state. The first shell distribution was isolated by back transforming the data with an R space window of 0.8–2.2 Å.

The RDF for both the solution and crystalline zinc enzymes are constructed using $Zn(Ac)_2(Im)_2$ as the reference compound (Figure 5A). There are small artifacts for the distribution, e.g., as the signal leakage for the second coordination shell at about 3 Å and the small negative distribution for the solution sample around 2.3 Å. The interference between the first and second coordination shells can be expected if the radial atomic distances are only 0.4 Å apart. Compared with the RDF of the model $Zn(Ac)_2(Im)_2$, the large peak in the RDF of solution ZnCPD reflects 4.2 atoms at an average distance of 2.03 Å and the small peak 1.2 atoms at 2.56 Å (integrated up to 2.9 Å). For the crystalline ZnCPD, however, the large peak reflects 4.0 atoms at 2.02 Å and the small peak 1.1 atoms at 2.38 Å (integrated up to 2.7 Å). The mean square displacements of the larger peaks for both the solution and crystalline samples are approximately the same, i.e., about 0.002 ± 0.001 Å^2 greater than the model compound.

The least-squares fitting method served to check the results of ZnCPD obtained by the RDF method. The fit was performed from 2.3 to 9.8 Å^{-1} in k space. Given that the R space window for isolating the first shell distribution is 1.4 Å in width, the data range used contains about seven degrees of freedom (Lee et al., 1981), which should be less than the number of variables used in the fitting procedure. A single-distance model, where a coordination number, a distance, and a Debye–Waller factor can be varied, yields Q values of 10.7 for the solution enzyme and 5.0 for the crystalline enzyme (Table II), indicating that this model should be rejected. The best fits from a two-distance fitting model, where two distances, two Debye–Waller factors, and one or two coordination numbers can be varied, are in excellent agreement with the experimental data for the solution and crystalline enzymes (Figure 6A,B). Calculation of Q from eq 1 gives a value of 0.4 for the solution enzyme and 0.6 for the crystalline enzyme, respectively (Table II). These results are consistent with the RDF results. Further use of a three-distance fit would not be justified since more than seven variables would have to be varied.

Table II: First Shell Fitting Results for ZnCPD and CoCPD

sample	form	modeling	N	R (Å)[a]	σ^2 (Å^2)	Q	status
ZnCPD	solution	one-distance	3.7	2.04	0.000	10.7	rejected
		two-distances	4	2.03 (1)	0.002	0.4	accepted
			1	2.57 (4)	0.000		
	crystals	one-distance	3.4	2.00	0.000	5.0	rejected
		two-distances	4	2.01 (1)	0.002	0.6	accepted
			1	2.36 (4)	0.002		
CoCPD	solution	one-distance	3.8	2.09	−0.001	9.8	rejected
		two-distances	4	2.08 (1)	0.002	0.6	accepted
			1	2.50 (4)	0.000		
	crystals	one-distance	4.8	2.12	0.008	4.3	rejected
		two-distances	4	2.10 (2)	0.004	2.1	?
			1	2.34 (8)	0.007		

[a] The value in the parentheses is ● the error in the last digit.

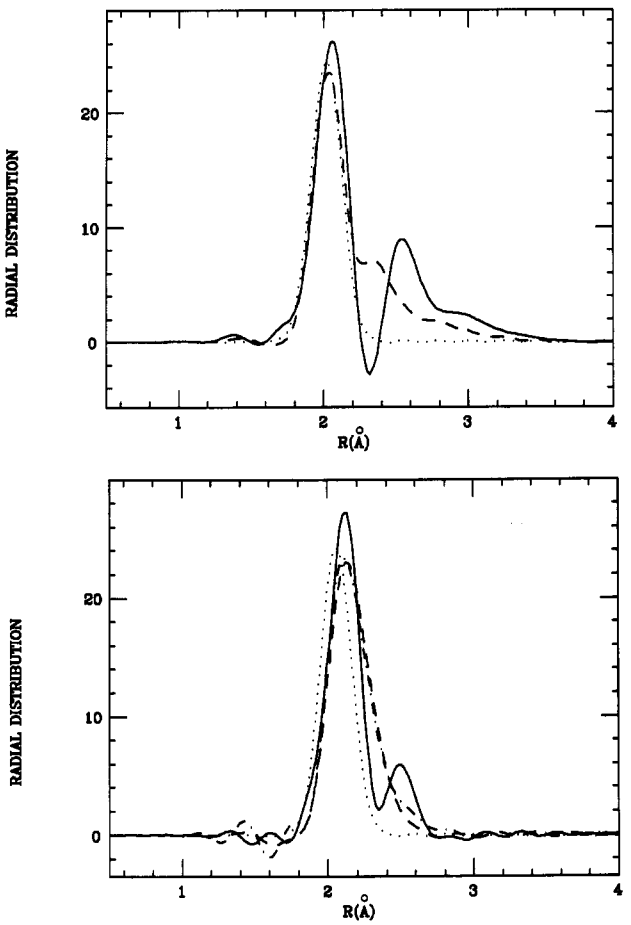

FIGURE 5: (A, top) RDFs of solution ZnCPD (solid) and crystalline ZnCPD (dash) compared with the RDF of $Zn(Ac)_2(Im)_2$ (dots). (B, bottom) RDFs of solution CoCPD (solid) and crystalline CoCPD (150 K, dash; 300 K, dot-dash) compared with the RDF of $Co(Ac)_2(Im)_2$ (dots). The distributions were broadened by a Gaussian factor of $\sigma_c^2 = 0.01$ Å^2 to reduce the truncation effects. The model compounds used are $Zn(Ac)_2(Im)_2$ and $Co(Ac)_2(Im)_2$ for Zn and Co enzymes, respectively.

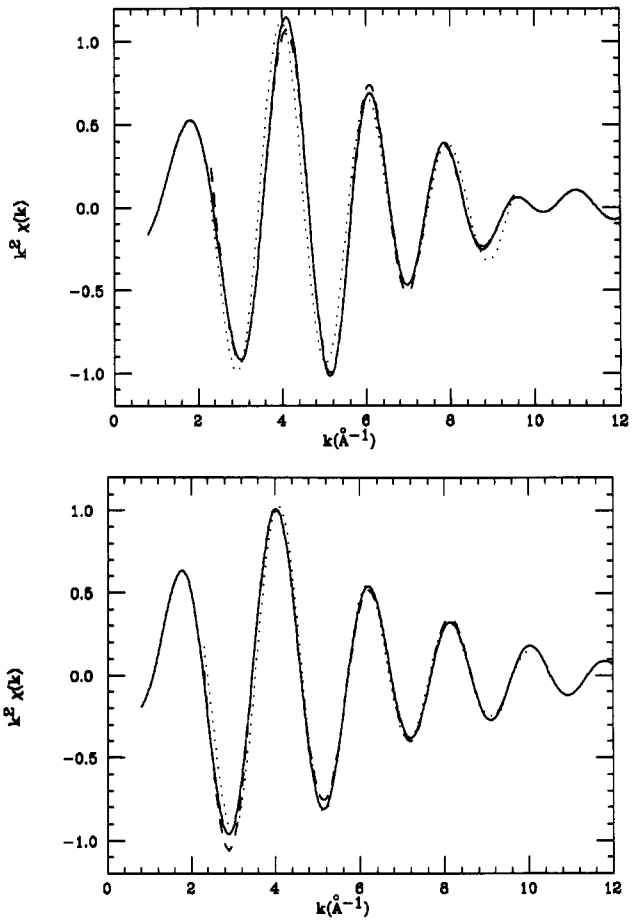

FIGURE 6: First shell $\chi(k)$ data of solution (A, top) and crystalline (B, bottom) ZnCPD (solid), compared with the single-distance fit (dot) and two-distance fit (dash). The data are weighted with a k^2 factor. According to the fitting criterion (see text), both single-distance fits can be rejected. These results are listed in Table II.

The same data analysis procedure was applied for CoCPD. The radial distribution functions of the solution and crystalline forms of the cobalt enzyme are compared to that for the Co complex $Co(Ac)_2(Im)_2$ (Figure 5B). Similar to ZnCPD, the RDF of the solution form of CoCPD consists of well-formed large and small peaks. Compared with the peak of $Co(Ac)_2(Im)_2$, the larger peak reflects about 4.3 atoms (O or N) at 2.08 Å and the smaller distribution reflects 0.9 atoms at 2.48 Å. The mean square displacement of the large peak is about the same as that for the model compound. For the crystalline form of CoCPD, however, the distribution is broad and contains 5.1 atoms (O or N) at an average distance of 2.15 Å. The mean square displacement of the distribution, subtracting out the Gaussian damping factor used to minimize the truncation effect in the transform, is about 0.009 Å^2.

The same fitting procedure and range in the k space were used for CoCPD. The error analysis again greatly favors the two-distance model for the cobalt enzyme in solution (Table II). However, there is no clear choice for the crystalline enzyme since the Q values are 4.3 and 2.1 for the one- and two-distance models, respectively. The reason that both fits are unsatisfactory can be explained by the RDF in Figure 5B. The distribution of the first coordination shell of Co in crystalline CoCPD is very disordered and non-Gaussian. Modeling

of the distribution with one or two Gaussian distributions is inappropriate. This illustrates one advantage of the RDF method.

In order to examine the effect of temperature on the first shell structural features in crystalline CoCPD, XAFS data were collected at 150 and 300 K (Figure 5B) and the results analyzed using the ratio method (Bunker, 1983). The logarithmic amplitude ratio and phase difference (not shown) between the first shell $\chi(k)$ data at these temperatures showed that the change of the coordination number is ≤ 0.2 and the average interatomic distance is within 0.01 Å, respectively. The Debye–Waller factor of the crystalline CoCPD at 300 K is about 0.001 ± 0.001 Å^2 larger than that at 150 K. This is consistent with the RDF generated for crystalline CoCPD at the two temperatures (Figure 5B). The RDF of crystalline CoCPD at 300 K is essentially the same in integrated area and average location as the RDF at 150 K (Figure 5B). The mean square displacement for the 300 K distribution is about 0.002 Å^2 larger than that at 150 K.

Higher Coordination Shells. The higher coordination shells in Zn- and Co-CPD were not susceptible to analysis with the accuracy of the present experimental procedure, except for the distribution located between 2.7 and 4.2 Å in the Fourier transform (Figure 4). This region is contributed mainly by γ-carbon and ϵ_2-nitrogen of the histidine located about 4 Å from the metal, which is enhanced about 3-fold due to the focusing effect (Bunker et al., 1982). The distribution was isolated using a back transform window of 2.7–4.2 Å for the enzymes and model compounds, $Co(Ac)_2(Im)_2$, $Zn(Ac)_2(Im)_2$, $Co(Im)_6$, and $Zn(Im)_4$. The least-squares fitting and the ratio method served to analyze these data using a short data range from 2 to 7 Å^{-1} in k space. The data at higher k are not reliable as indicated by the variation of the spectrum from scan to scan. The analysis of $Co(Ac)_2(Im)_2$ and $Zn(Ac)_2(Im)_2$ using the imidazole models indicated about two imidazoles for both cases, suggesting that the γ-carbon and δ_2-nitrogen indeed are mainly the ones that contribute to the distribution. The experimental data of the Co and Zn enzymes were modeled by $Co(Ac)_2(Im)_2$ and $Zn(Ac)_2(Im)_2$, respectively. For crystalline and solution ZnCPD, two imidazole rings were found for the distribution, with a disorder similar to that measured by the Debye–Waller factor. The average interatomic distance between Zn and its surrounding ligating atoms for ZnCPD in solution is about 0.06 ± 0.04 Å greater than both its crystalline counterpart and the model. Similar to the Zn enzyme, the higher coordination shell of solution and crystalline CoCPD consists of two imidazoles located at about 0.07 ± 0.04 Å farther away from the metal ion than that of the model $Co(Ac)_2(Im)_2$. The distribution of the crystalline enzyme was greatly disordered but that for the solution enzyme was not. The amplitude of $\chi(k)$ of the crystalline CoCPD decreases significantly at the high k region relative to that of CoCPD in solution (Figure 7). The reduction corresponds to a Debye–Waller factor σ^2 of 0.009 ± 0.002 Å^2 in a Gaussian model. This finding not only is consistent with the large first shell disorder in the crystals but also provides information for the distribution of the nitrogen ligands of the two histidines.

The Near Edge Region. The 3d "pip", which is the pre-edge bump, is caused by the electron transition from a 1s state to unoccupied 3d states. With a filled 3d shell, the absorption spectrum of zinc ion has no 3d pip feature, but this is present for cobalt. This quadrupole transition is usually weak but can be enhanced by breaking of the inversion symmetry of the metal ion, which allows dipole transitions (Schulman et al., 1976). Thus, a transition of an orthorhombic to a tetragonal

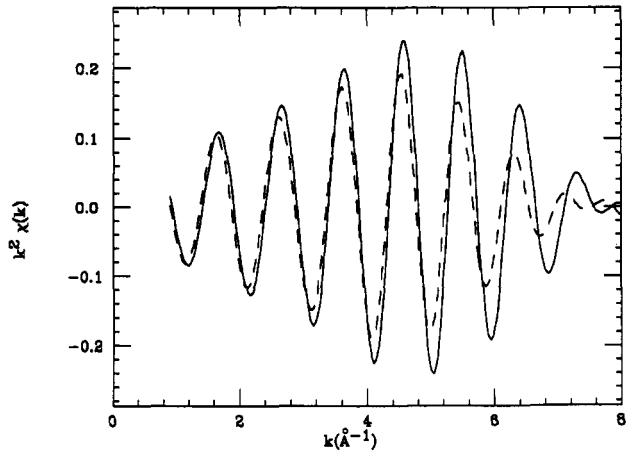

FIGURE 7: XAFS $\chi(k)$ data of the third shell of CoCPD solution sample (solid) and CoCPD crystlline sample (dash). The data are weighted with a k^2 factor. The contributions were isolated between 2.8 and 4.2 Å in the Fourier transforms of Figure 4B. The signal is mainly due to the γ-carbon and δ_1-nitrogen of the histidines.

metal environment will enhance the 3d pip intensity. The 3d pip intensity was measured relative to the absorption edge step for Co model compounds and the proteins. For the model compounds with orthorhombic metal coordination (Wyckoff, 1963), such as cobalt acetate, cobalt carbonate, and $Co(Im)_6$, the intensities are 0.041, 0.040, and 0.037 with an error of 0.003, respectively. For the model with tetragonal metal environment, $Co(Ac)_2(Im)_2$, the 3d pip is 0.085 ± 0.003. The 3d pip intensity for solution CoCPD is 0.081 ± 0.004, indicating a slightly distorted tetragonal metal site. The intensity of crystalline CoCPD is 0.068 ± 0.004, which is further distorted from its solution counterpart. This would be expected if the first shell of crystalline CoCPD is more likely a pentacoordinated site.

Discussion

Radiation damage to a biological sample by intense X-ray radiation from a synchrotron source has been observed (Chance et al., 1980). We tried to minimize the damage in two ways. One is to use concentrated samples (usually 2–2.5 mM) to reduce the data collection time and therefore to reduce the length of exposure of the sample to the X-ray beam. The other is to perform the experiment at low temperatures (usually about 130 K) to minimize reduction of the sample by hydrated electrons. The sample integrity of the enzyme was checked after the XAFS experiment by amino acid analysis and activity measurements. Unusual amino acids were not observed, and the composition of the protein was essentially unchanged. The specific activity of the enzyme was not altered under the present conditions of X-ray radiation. The integrity of the samples was also monitored directly by the repeatability of the XAFS spectrum. Progressive changes with time were not observed during the measurements.

Other means may also affect the sample. Thus, the storage of the enzyme in dry ice causes XAFS spectral changes which may be due to the reaction of CO_2 with the active site of the protein and was therefore avoided in the present study. Nearly all our enzyme and model compounds were measured two or more times over different time intervals, to eliminate systematic experimental efforts.

We have adopted the radial distribution function method (splice method) as a reference for the analysis of these data. The method does not require an assumed form of the distribution of atoms, such as sums of Gaussian shells. Therefore, it reduces the biased errors which a false structural model can

introduce in the least-squares fitting method. As a matter of fact, we could not obtain a satisfactory fit for the solution data using the X-ray diffraction results as a starting model in the fitting procedure until the RDF was generated to provide a correct model. However, the fitting method is still useful to obtain more precise results and is easier for the performance of error analysis. The fitting criterion used for error analysis incorporated the variations of measurement and modeling errors in k space, which has been recommended (Report of the International Workshop on Standards and Criteria in XAFS, 1989).

The XAFS data analysis shows that the first shell of carboxypeptidase A contains five atoms (O or N) for both solution and crystalline forms and in Zn and Co enzymes. Differences between interatomic distances of solution and crystals are found for both the Zn and Co enzymes (Table II). For the Zn protein in solution, four atoms are at 2.03 ± 0.01 Å, and one atom is at 2.57 ± 0.04 Å. For the crystalline enzyme, the four atoms are at 2.01 ± 0.01 Å, but one atom is at 2.36 ± 0.04 Å. On the basis of the fact that the zinc is bound to His-69, His-196, Glu-72, and a water molecule, a suitable structural model of the metal coordination site in ZnCPD can be proposed which is consistent with existing data. The four atoms at an average distance of 2.03 Å are assigned to two δ_1-nitrogens of His-69 and His-196, one ϵ_1-oxygen of Glu-72, and the oxygen of the water. Since the Debye–Waller factor σ^2 of the four-atom distribution is relatively small ($\leq$0.003 Å^2), the spread of the four distances should also be small. Assuming a two-atom and a two-distance separation, this disorder allows the difference of the two distances to be about 0.11 Å apart. The fifth atom at 2.57 Å of ZnCPD in solution is assigned to the ϵ_2-oxygen of Glu-72. The above structural model is based on the following considerations. First, the two nitrogens of His-69 and His-196 are contained in the four-atom distribution as demonstrated by the results of the higher coordination shell analysis. Alternatively, we can assign the fifth atom at 2.57 Å to the oxygen of the water molecule, and both ϵ_1- and ϵ_2-oxygens are then bound to the zinc ion at an average distance of 2.03 Å from the zinc ion. However, this type of coordination of Glu-72 would place the γ-carboxylate carbon at a distance of 2.3 Å from the metal. Since this γ-carbon was not seen, this alternative model of Glu-72 coordination can be rejected. On crystallization of the Zn enzyme, the four-atom distribution in solution remained the same, while the ϵ_2-oxygen moved about 0.2 Å closer to the metal. This can be interpreted as a rotation of Glu-72 upon crystallization. Given that the ϵ_1-oxygen is a pivot point for the rotation and all the bonds and angles of Glu-72 are unchanged, the rotation will translate to a main chain movement of approximately 0.4 Å.

If comparisons are made between the Zn and Co enzymes in solution, slight differences in metal–ligand distances are observed. Thus the average distance of the four-atom distribution for the Co enzyme is 0.04 Å greater than that for the Zn enzyme (Table II), a value that is in the same order (Co > Zn) and range (0.03–0.05 Å) observed for the ligand distances of the Zn and Co diimidazole and dialkyl carboxylate complexes as determined by X-ray diffraction (Horrocks et al., 1980).

The same structural model adequately describes the active site structure of the cobalt enzyme in solution. The four atoms, two δ_1-nitrogens of His-69 and His-196, one ϵ_1-oxygen of Glu-72, and the oxygen of the water, are at an average distance of 2.08 Å. The ϵ_2-oxygen of Glu-72 is located at 2.50 Å. It can be anticipated that a similar rotation of Glu-72 of ZnCPD has occurred in CoCPD upon crystallization since the fifth atom is found at 2.34 Å in the crystalline state. However, the crystalline state of CoCPD differs significantly from that of ZnCPD, characterized particularly by the large disorder observed for CoCPD. Ligand(s) other than the ϵ_2-oxygen of Glu-72 must also contribute to the disorder. Higher shell data analysis of CoCPD indicate that the two histidine in the crystalline state are disordered more radially than in solution state, contributing to the first coordination shell disorder.

Table III: X-ray Crystallographic Results of Metal–Ligand Distances of Carboxypeptidase A[a]

samples	R	Nδ_1	Nδ_1	Oϵ_1	H_2O	average	Oϵ_2
ZnCPD[b]	1.54	2.17	2.03	2.19	2.19	2.15	2.30
ZnCPD[c]	1.54	2.13	2.07	2.17	2.01	2.10	2.31
ZnCPD[d]	1.75	2.10	2.08	2.23	1.96	2.09	2.33
CoCPD[b]	1.7	2.13	2.06	2.24	2.00	2.11	2.26

[a] All distances and the resolution level R are in Angstroms. The average distance is calculated for the two δ_1 nitrogens of His-69 and His-196, the ϵ_1 oxygen of Glu-72, and the oxygen of the water molecule. [b] Hardman and Lipscomb (1984). [c] Rees et al. (1986). [d] Rees et al. (1981).

The RDF for the cobalt crystals at 150 and 300 K are essentially superimposable, indicating there are no detectable conformational differences in the crystals at these two widely different temperatures (Figure 5B). The Debye–Waller factor increase of 0.002 Å^2 from 150 to 300 K reflects the expected increase of thermal disorder at the higher temperature. The analysis of ZnCPD·L-Phe complex at 150 and 300 K for the zinc first coordination shell indicates that the coordination number and the interatomic distance were the same and that the first shell distribution at 300 K shows an increased disorder (unpublished results). These observations further suggest that the structure of solution and crystalline carboxypeptidase remains unchanged from 150 to 300 K.

X-ray crystallographic measurements on carboxypeptidase A have been refined to 1.54-Å resolution for the zinc enzyme and 1.7-Å resolution for the Co enzyme (Rees et al., 1983; Hardman et al., 1984). The results for the metal–ligand distances are listed in Table III. Although the results for CoCPD (five atoms at 2.14 Å with σ^2 = 0.010 Å^2) are consistent with our crystalline results, the X-ray data for ZnCPD are quite different from those by XAFS on ZnCPD crystals. In X-ray diffraction the average distance for the two nitrogens of His-69 and His-196, the ϵ_1-oxygen of Glu-72, and the oxygen of the water is 2.15 Å (Hardman & Lipscomb, 1984), 2.10 Å (Rees et al., 1986), or 2.09 Å (Rees et al., 1981), compared to 2.01 Å determined by XAFS for the ZnCPD crystalline sample; and the ϵ_2-oxygen of Glu-72 is at 2.30–2.33 Å by X-ray diffraction (Table III), as compared to 2.36 Å from XAFS. The structural disorder for the four-atom distribution determined by X-ray diffraction is 0.005 Å^2, slightly greater than that determined by XAFS (0.002 Å^2).

The differences from a general comparison of results from XAFS performed on solution and X-ray crystallography, respectively, can be conjectured to arise from two possible sources. One could be due to errors associated with the poor accuracy of X-ray crystallography on large molecules, while the other could be the differences between crystalline and solution states. For met-myoglobin, both possibilities have been shown to exist (Zhang et al., 1991). X-ray crystallography can provide tremendous amounts of information of the three-dimensional structure of proteins and has been proven to be essential for the understanding of the function of many proteins. XAFS, on the other hand, is only sensitive to the first few coordination shells surrounding the metal ion and

provides comparatively limited structural information. However, XAFS is believed to be more detailed and accurate than X-ray crystallography, specifically for the metal environment of large molecules. A direct comparison of the results from the two techniques can provide an error estimation on the active site structure for diffraction, which is difficult to perform in X-ray crystallographic refinement for large molecules. In this regard the two structural techniques complement one another.

Regardless of the merits of X-ray diffraction versus XAFS, it seems clear that telling structural differences arise at the active site of the carboxypeptidase A upon crystallization. Thus, while XAFS did not reveal any difference for ZnCPD crystallized from NaCl and LiCl, it does demonstrate differences in the active site structure of crystalline ZnCPD from that of its form in solution. Kinetic and spectroscopic studies on both solution and crystalline forms of carboxypeptidase A indicate differences between the two forms of the enzyme (Johansen & Vallee, 1975; Spilburg et al., 1974, 1977; Scheule et al., 1980; Bachovchin et al., 1982; Vallee et al., 1983). However, the questions relative to the identity of the two forms of the enzyme have remained unanswered due to the lack of structural information on the solution state. For the first time, we here report structural differences observed at the active sites of solution and crystalline CoCPD and ZnCPD. On the basis of the X-ray crystallographic studies on different crystal forms of the zinc enzyme (Kim & Lipscomb, 1990), it was inferred that crystal packing forces in these structures impose little influence on the tertiary structure of the enzyme, which was taken as evidence of structural identity between solution and crystalline states. Our XAFS study indicates that this is an overgeneralization.

The structures of the solution forms of ZnCPD and CoCPD are quite similar, as might be expected since the enzymes share similar catalytic properties (Auld & Vallee, 1970, 1971; Latt & Vallee, 1971; Auld et al., 1984). On the basis of the structural model proposed, it can be speculated that the structural changes between solution and crystalline forms of the enzyme could affect the catalytic activity of the crystalline enzyme in two ways. First, the movement of ϵ_2-oxygen of Glu-72 0.2 Å closer to the zinc could affect the coordination geometry of the metal ion, changing its properties for substrate binding and catalysis. Second, the rotation of Glu-72 in crystals may be accompanied by a conformational change at the active site and/or in the protein as a whole which could in turn affect the binding of inhibitors and substrates to the crystal. Such questions in relation to the binding of substrates and inhibitors of carboxypeptidase in the solution state deserve further inquiry.

ACKNOWLEDGMENTS

We appreciate the support of the staff of the NBPRT beamline X9-A and National Synchrotron Light Source.

REFERENCES

Auld, D. S (1988) *Methods Enzymol. 158*, 71.
Auld, D. S., & Vallee, B. L. (1970) *Biochemistry 9*, 4352.
Auld, D. S., & Vallee, B. L. (1971) *Biochemistry 10*, 2892.
Auld, D. S., & Vallee, B. L. (1987) in *Hydrolytic Enzymes* (Neuberger, A., & Brocklehurst, K., Eds.) pp 201–255, Elsevier, New York.
Auld, D. S., Galdes, A., Geoghegan, K. F., Holmquist, B., Martinelli, R. A., & Vallee, B. L. (1984) *Proc. Natl. Acad. Sci. U.S.A. 81*, 5041.
Bachovchin, W. W., Kanamori, K., Vallee, B. L., & Roberts, J. D. (1982) *Biochemistry 21*, 2855.
Bicknell, R., Schäffer, A., Bertini, I., Luchinat, C., Vallee, B. L., & Auld, D. S. (1988) *Biochemistry 27*, 1050–1057.
Bidlingmeyer, B. A., Cohen, S. A., & Tarvin, T. L. (1984) *J. Chromatogr. 336*, 93.
Bouldin, C. E. (1984) Ph.D. Thesis, University of Washington, Seattle, WA.
Bradshaw, R. A., Ericsson, L. H., Walsh, K. A., & Neurath, H. (1969) *Proc. Natl. Acad. Sci. U.S.A. 63*, 1389.
Bunker, G. (1983) *Nucl. Instrum. Methods 207*, 437.
Bunker, G., Stern, E. A., Blankenship, R. E., & Parson, W. W. (1982) *Biophys. J. 37*, 539.
Chance, B., Angiolillo, P., Yang, E. K., & Powers, L. (1980) *FEBS Lett. 112*, 178.
Christianson, D. W., & Lipscomb, W. N. (1989) *Acc. Chem. Res. 22*, 62.
Coleman, J. E., Allen, B. J., & Vallee, B. L. (1960) *Science 131*, 350.
Cox, D. J., Bovard, F. C., Bargetzi, J.-P., Walsh, K. A., & Neurath, H. (1964) *Biochemistry 3*, 44.
Crozier, E. D., Rehr, J. J., & Ingalls, R. R. (1988) in *X-ray Absorption: Principle, Application, Techniques of EXAFS, SEXAFS, and XANES* (Koningsberger, D. C., & Prins, R. Eds.) p 373, John Wiley and Sons, New York.
Davis, W. J., & Smith, J. (1971) *J. Chem. Soc. A*, 317.
Furey, W. F., Robbins, A. H., Clancy, L. L., Winge, D. R., Wang, B. C., & Stout, C. D. (1987) in *Metallothionein II* (Kägi, J. H. R., & Kojima, Y., Eds.) pp 139–148, Birkhäuser, Verlag, Basel, Switzerland.
Geogheghan, K., Holmquist, B., Spilburg, C., & Vallee, B. L. (1983) *Biochemistry 22*, 1847–1852.
Hardman, K. D., & Lipscomb, W. N. (1984) *J. Am. Chem. Soc. 106*, 463.
Hilvert, D., Gardell, S. J., Rutter, W. J., & Kaiser, E. T. (1986) *J. Am. Chem. Soc. 108*, 5298.
Holmquist, B. (1988) *Methods Enzymol. 158*, 6.
Horrocks, W. DeW., Jr., Ishley, J. N., Holmquist, B., & Thompson, J. S. (1980) *J. Inorg. Biochem. 12*, 131.
Johansen, J. T., & Vallee, B. L. (1975) *Biochemistry 14*, 649.
Kim, H., & Lipscomb, W. N. (1990) *Biochemistry 29*, 5546.
Laemmli, U. K. (1970) *Nature (London) 227*, 680.
Larsen, K. S., & Auld, D. S. (1989) *Biochemistry 28*, 9620.
Latt, S. A., & Vallee, B. L. (1971) *Biochemistry 10*, 4263.
Lee, P. A., Citrin, P. H., Eisengberger, P., & Kincaid, B. M. (1981) *Rev. Mod. Phys. 53*, 769.
Lin, S., Stern, E. A., Kalb (Gilboa), A. J., & Zhang, Y. (1990) *Biochemistry 29*, 3599.
Lin, S., Stern, E. A., Kalb (Gilboa), A. J., & Zhang, Y. (1991) *Biochemistry 30*, 2323.
Lipscomb, W. N., Hartsuck, J. A., Reeke, G. N., Quiocho, F. A., Bethge, P. H., Ludwig, M. L., Steitz, T. A., Muirhead, H., & Coppola, J. C. (1968) *Brookhaven Symp. Biol. 21*, 24.
Lipscomb, W. N., Reeke, G. N., Hartsuck, J. A., Quiocho, F. A., & Bethge, P. H. (1970) *Phil Trans. R. Soc. London 257*, 17.
Messerle, B. A., Schäffer, A., Vašák, M., Kägi, J. H. R., & Wüthrich, K. (1990) *J. Mol. Biol. 214*, 765.
Neurath, H., Bradshaw, R. A., Petra, P. H., & Walsh, K. A. (1970) *Phil. Trans. R. Soc. London Ser. B 257*, 177.
Quiocho, F. A., & Lipscomb, W. N. (1971) *Adv. Protein Chem. 25*, 1.
Reeke, G. N., Hartsuck, J. A., Ludwig, M. L., Quiocho, F. A., Steitz, T. A., & Lipscomb, W. N. (1967) *Proc. Natl. Acad. Sci. U.S.A. 58*, 2220.

Rees, D. C., Lewis, M., Honzatko, R. B., Lipscomb, W. N., & Hardman, K. D. (1981) *Proc. Natl. Acad. Sci. U.S.A. 78*, 3405.
Rees, D. C., Lewis, M., Honzatko, R. B., & Lipscomb, W. N. (1983) *J. Mol. Biol. 168*, 367.
Rees, D. C., Howard, J. B., Chakrabarti, P., Yeates, T., Hsu, B. T., Hardman, K. D., & Lipscomb, W. N. (1986) in *Zinc Enzymes* (Bertini, I., Luchinat, C., Maret, W., & Zeppezauer, M., Eds.) pp 155-166, Birkhaüser, Boston, MA.
Report of International Workshop on Standards and Criteria in X-Ray absorption Spectroscopy (1989) *Physica B. 158*, 709.
Riordan, J. F., & Holmquist, B. (1984) in *Methods of Enzymatic Analysis* (Bermeyer, H. O., Ed.) 3rd ed., Vol. 5, pp 44-60, Verlag Chemie, Weinheim, FRG.
Scheule, R. K., Van Wart, H. E., Vallee, B. L., & Scheraga, H. A. (1980) *Biochemistry 19*, 759.
Schulze, P., Wörgötter, E., Braun, W., Wagner, G., Vašák, M., Kägi, J. H. R., & Wüthrich, K. J. (1988) *J. Mol. Biol. 203*, 251.
Schulman, R. T., Yafet, Y., Eisenberger, T., & Blumberg, W. E. (1976) *Proc. Natl. Acad. Sci. U.S.A. 73*, 1384.
Smith, S. O., Farr-Jones, S., Griffen, R. G., & Bachovchin, W. W. (1989) *Science 244*, 961.
Spilburg, C. A., Bethune, J. L., & Vallee, B. L. (1974) *Proc. Natl. Acad. Sci. U.S.A. 71*, 3922.
Spilburg, C. A., Bethune, J. L., & Vallee, B. L. (1977) *Biochemistry 16*, 1142.
Stern, E. A., & Heald, S. M. (1983) in *Handbook on Synchrotron Radiation* (Koch, E. E., Ed.) pp 955-1014, North-Holland, New York.
Uren, J. R., & Neurath, H. (1972) *Biochemistry 11*, 4483.
Vallee, B. L., & Neurath, H. (1954) *J. Am. Chem. Soc. 76*, 5006.
Vallee, B. L., & Auld, D. S. (1990) *Biochemistry 29*, 5647.
Vallee, B. L., Riordan, J. F., & Coleman, J. E. (1963) *Proc. Natl. Acad. Sci. U.S.A. 49*, 109.
Vallee, B. L., Riordan, J. F., Auld, D. S., & Latt, S. A. (1970) *Phil. Trans. R. Soc. London Ser. B 257*, 215.
Vallee, B. L., Galdes, A., Auld, D. S., & Riordan, J. F. (1983) in *Zinc Enzymes* (Spiro, T. G., Ed.) Chapter 2, John Wiley and Sons, New York.
Wyckoff, R. W. G. (1963) *Crystal Structures*, 2nd ed., Interscience, NY.
Zhang, K., Stern, E. A., Ellis, F., Sanders-Loehr, J., & Shiemke, A. K. (1988) *Biochemistry 27*, 7470.
Zhang, K., Chance, B., Reddy, K. S., Ayene, I., Stern, E. A., & Bunker, G. (1991) *Biochemistry 30*, 9116.

pH Dependence of the Interaction of Hirudin with Thrombin

Andreas Betz, Jan Hofsteenge, and Stuart R. Stone*,‡
Friedrich Miescher-Institut, P.O. Box 2543, CH-4002 Basel, Switzerland
Received July 1, 1991; Revised Manuscript Received October 24, 1991

ABSTRACT: The kinetics of the inhibition of human α-thrombin by recombinant hirudin have been studied over the pH range from 6 to 10. The association rate constant for hirudin did not vary significantly over this pH range. The dissociation constant of hirudin depended on the ionization state of groups with pK_a values of about 7.1, 8.4, and 9.2. Optimal binding of hirudin to thrombin occurred when the groups with pK_a values of 8.4 and 9.0 were protonated and the other group with a pK_a of 7.1 was deprotonated. The pH kinetics of genetically engineered forms of hirudin were examined in an attempt to assign these pK_a values to particular groups. By using this approach, it was possible to show that protonation of His51 and ionization of acidic residues in the C-terminal region of hirudin were not responsible for the observed pK_a values. In contrast, the pK_a value of 8.4 was not observed when a form of hirudin with an acetylated α-amino group was examined, and, thus, this pK_a value was assigned to the α-amino group of hirudin. The requirement for this group to be protonated for optimal binding to thrombin is discussed in terms of the crystal structure of the thrombin-hirudin complex. Examination of this structure allowed the other pK_a values of 7.1 and 9.2 to be tentatively attributed to His57 and the α-amino group of Ile16 of thrombin.

Hirudin was originally isolated from the leech as a specific inhibitor of thrombin (Markwardt, 1970). The major form of hirudin is 65 amino acids in length (Bagdy et al., 1976; Dodt et al., 1984) and is composed of an N-terminal core region held together by 3 disulfide bonds and a flexible C-terminal tail (Folkers et al., 1989; Haruyama & Wüthrich, 1989). Hirudin inhibits thrombin by a unique mechanism. The three N-terminal residues of hirudin are bound in the active-site cleft of thrombin, but the orientation of the polypeptide chain of hirudin within the active site is opposite to that observed with other proteinase inhibitors. Moreover, hirudin does not bind to the primary specificity pocket of thrombin. Hirudin uses binding sites removed from the catalytic center in order to achieve a specific interaction with thrombin. In particular, the C-terminal region of thrombin is bound to a positively charged surface groove on thrombin that has been called the anion-binding exosite (Rydel et al., 1990; Grütter et al., 1990).

The kinetic mechanism for the inhibition of thrombin by hirudin involves at least two steps. The first step, which is rate-determining with picomolar concentrations of hirudin, does not involve the binding of hirudin to the active site of thrombin. In a subsequent step, hirudin binds at the active site to form a tighter complex (Stone & Hofsteenge, 1986; Stone et al., 1987). In the present study, the kinetic mechanism of the interaction of hirudin with thrombin has been

* Correspondence should be addressed to this author.
‡ Present address: Department of Haematology, University of Cambridge, MRC Centre, Hills Road, Cambridge CB2 2QH, United Kingdom.

0006-2960/92/0431-1168$03.00/0